

Article

The Mechanism of the Formation of the Spin Hall Effect in a Sharp Focus

Victor V. Kotlyar ^{1,2} , Sergey S. Stafeev ^{1,2,*} , Alexey M. Telegin ^{1,2} and Elena S. Kozlova ^{1,2}

¹ Laser Measurements Laboratory, IPSI RAS—Branch of the FSRC “Crystallography and Photonics” RAS, 443001 Samara, Russia; kotlyar@ipsiras.ru (V.V.K.); telegin.am@ssau.ru (A.M.T.); kozlova.es@ssau.ru (E.S.K.)

² Technical Cybernetics Department, Samara National Research University, 443086 Samara, Russia

* Correspondence: sergey.stafeev@gmail.com

Abstract: We have shown how the spin Hall effect is formed in a tight focus for two light fields with initial linear polarization. We have demonstrated that an even number of local subwavelength regions appear in which the sign of the longitudinal projection of the spin angular momentum (the third Stokes component) alternates. When an optical vortex with topological charge n and linear polarization passes through an ideal spherical lens, additional optical vortices with topological charges $n + 2$, $n - 2$, $n + 1$, and $n - 1$ with different amplitudes are formed in the converged beam. The first two of these vortices have left and right circular polarizations and the last two vortices have linear polarization. Since circularly polarized vortices have different amplitudes, their superposition will have elliptical polarization. The sign of this elliptical polarization (left or right) will change over the beam cross section with the change in the sign of the difference in the amplitudes of optical vortices with circular polarization. We also have shown that optical vortices with topological charges $n + 2$, $n - 2$ propagate in the opposite direction near the focal plane, and together with optical vortices with charges $n + 1$, $n - 1$, they form an azimuthal energy flow at the focus.

Keywords: optical vortex; optical Hall effect; cylindrical vector beam; Richards–Wolf formula



Citation: Kotlyar, V.V.; Stafeev, S.S.; Telegin, A.M.; Kozlova, E.S.

The Mechanism of the Formation of the Spin Hall Effect in a Sharp Focus. *Photonics* **2023**, *10*, 1093. <https://doi.org/10.3390/photonics10101093>

Received: 7 September 2023

Revised: 25 September 2023

Accepted: 28 September 2023

Published: 29 September 2023



Copyright: © 2023 by the authors. Licensee MDPI, Basel, Switzerland. This article is an open access article distributed under the terms and conditions of the Creative Commons Attribution (CC BY) license (<https://creativecommons.org/licenses/by/4.0/>).

1. Introduction

The photonic (or optical) spin Hall effect is a fundamental optical phenomenon that occurs after the propagation of a beam of light through an optical interface or an inhomogeneous medium. It represents the spin-dependent deviation of the real photon path from the geometric propagation path. The optical spin Hall effect was first predicted in [1]. In this work, a semiclassical equation of the motion of a wave packet of light was obtained, taking into account the Berry curvature in momentum space. This equation naturally describes the interaction between orbital and spin angular momentum, i.e., the conservation of the total angular momentum of light. This leads to a shift in the motion of the wave packet perpendicular to the permittivity gradient, i.e., to the polarization-dependent Hall effect for light. Later, also theoretically, in [2], the spin Hall effect was demonstrated during the refraction and reflection of a linearly polarized Gaussian beam at the interface between two media. In [2], the transverse displacements of the centers of the beams were calculated. When a linearly polarized light beam is scattered, photons of opposite helicity accumulate at opposite borders of the beam. Later, the optical spin Hall effect was also predicted in [3] for the Rayleigh scattering of light in a microcavity. In [3], an analogy was established between the well-known spin Hall effect in semiconductors and the polarization dependence of Rayleigh light scattering in microcavities. This dependence is a consequence of the strong spin effect during the elastic scattering of exciton–polaritons: if the initial polariton state has zero spin and is characterized by linear polarization, the scattered polaritons become strongly spin-polarized. The polarization in the scattered state can be positive or negative, depending on the orientation of the linear polarization of the initial state

and the scattering direction. The spin polarizations of polaritons scattered clockwise and counterclockwise have different signs. In [4], the experimental observation of the existence of the optical spin Hall effect was reported and the propagation of polariton spin over more than 100 μm in a high-quality quantum microcavity in the GaAs/AlGaAs structure was demonstrated. When the polarization plane of the exciting light rotated, the direction of the spin was switched. In [4], the light leaving the microcavity formed four side lobes in the far diffraction zone, two of which had right-hand circular polarization along one diagonal and left-hand circular polarization along the other diagonal. If a transverse electric polarization was chosen instead of the transverse magnetic polarization, then the left- and right-hand polarizations in the far zone were changed. It was experimentally shown [5] that when light with linear polarization propagates through a hyperbolic metasurface (the metasurface has different dielectric transmission in different directions), light with right and left circular polarization will be collected at the borders of the laser beam. In [5], a binary subwavelength grating in a thin gold film on the glass surface was used as a hyperbolic metasurface. The grating period was 220 nm, the height was 50 nm, and the wavelength was 532 nm and 638 nm. To demonstrate the Hall effect, the third component of the Stokes vector was measured.

In [6,7], the spin Hall effect was also investigated in other metalenses. For example, in [7], the metasurface consisted of V-shaped gold antennas located on a transparent substrate. By changing the length and orientation of the V-shaped structures of subwavelength antennas with a size of 180 nm, tunable phase delays were introduced between the incident field with a telecommunication wavelength and linear polarization and the first order of diffraction. In the far zone of the transmitted beam, the spin Hall effect was observed, since light with left and right circular polarizations propagated at different angles to the optical axis. In [8], a review is given of papers on the optical spin Hall effect, which also arises in chiral materials [9], multilayer nanostructures [10], two-dimensional atomic crystals (graphene) [11,12], and topological materials [13].

In the above-mentioned papers, special, complex, and exotic optical elements were fabricated to demonstrate the spin Hall effect. However, the spin Hall effect arises in simpler situations, for example, when light passes through an ordinary spherical lens [14–16]. To increase the effect, spherical lenses with a high numerical aperture are required. Even more simply, the spin Hall effect was experimentally demonstrated in paraxial laser beams with a special type of cylindrical polarization, which had only linear polarization in the initial plane at each point [17]. In paraxial beams, the Hall effect arises due to diffraction in free space and is much stronger than in the case of refraction at the interface.

In this work, using two initial vortex laser beams with homogeneous and non-uniform linear polarization, the mechanism of the formation of the spin Hall effect in a tight focus is investigated. The Richards–Wolf theory [18] makes it possible to obtain exact analytical expressions in the focus for all projections of the vectors of the electric and magnetic fields of an electromagnetic wave. By analyzing the obtained expressions, it was shown that when a light beam passes through the focus of a spherical lens, there is a spatial separation of light with right and left elliptical polarization.

2. Additional Optical Vortices Formed after a Spherical Lens

We investigated an optical vortex with linear polarization with the initial Jones vectors:

$$\mathbf{E}(\theta, \varphi) = A(\theta) \exp(in\varphi) \begin{pmatrix} 1 \\ 0 \end{pmatrix}, \quad \mathbf{H}(\theta, \varphi) = A(\theta) \exp(in\varphi) \begin{pmatrix} 0 \\ 1 \end{pmatrix}, \quad (1)$$

where θ is the polar angle; φ is the azimuthal angle, which defines a point on a sphere with the center in the focus; and n is the topological charge, an integer, and the linear polarization

vector is directed along the horizontal x -axis. In [19], the projections of the electric and magnetic vectors in the plane of tight focus for the initial field (1) were obtained:

$$\begin{aligned}
 E_x &= \frac{i^{n-1}}{2} e^{in\varphi} (2I_{0,n} + e^{2i\varphi} I_{2,n+2} + e^{-2i\varphi} I_{2,n-2}), \\
 E_y &= \frac{i^n}{2} e^{in\varphi} (e^{-2i\varphi} I_{2,n-2} - e^{2i\varphi} I_{2,n+2}), \\
 E_z &= i^n e^{in\varphi} (e^{-i\varphi} I_{1,n-1} - e^{i\varphi} I_{1,n+1}), \\
 H_x &= \frac{i^n}{2} e^{in\varphi} (e^{-2i\varphi} I_{2,n-2} - e^{2i\varphi} I_{2,n+2}), \\
 H_y &= \frac{i^{n-1}}{2} e^{in\varphi} (2I_{0,n} - e^{2i\varphi} I_{2,n+2} - e^{-2i\varphi} I_{2,n-2}), \\
 H_z &= i^{n+1} e^{in\varphi} (e^{-i\varphi} I_{1,n-1} + e^{i\varphi} I_{1,n+1}).
 \end{aligned}
 \tag{2}$$

Equation (2) includes functions $I_{\nu, \mu}$ that depend only on the radial variable r :

$$I_{\nu, \mu} = 2kf \int_0^\alpha \sin^{\nu+1} \left(\frac{\theta}{2} \right) \cos^{3-\nu} \left(\frac{\theta}{2} \right) \cos^{1/2}(\theta) A(\theta) e^{ikz \cos \theta} J_\mu(kr \sin \theta) d\theta,
 \tag{3}$$

where $k = 2\pi/\lambda$ is the wave number of monochromatic light with wavelength λ ; f is the focal length of the lens; α is the maximum angle of the inclination of rays to the optical axis, which is determined by the numerical aperture of the aplanatic lens $NA = \sin \alpha$; and $J_\nu(\xi)$ is the Bessel function of the first kind of the ν^{th} order. The function $A(\theta)$ is a real function that determines the radially symmetric amplitude of the initial field, which depends on the angle of inclination θ of the beam emanating from a point on the initial spherical front and converging to the center of the focus plane. The description of the light field at the focus using Equation (3) was first obtained in the classic work by Richards and Wolf [18].

It should be noted that in this paper, expressions (2) are correct near the focal plane and in the focus located at $z = 0$. Therefore, when in this work we talk about focus, it means that we talk about the field in the focal plane ($z = 0$).

It can be seen from (2) that although the initial field has one optical vortex with topological charge n and amplitude $\exp(in\varphi)$, the focal plane contains four optical vortices with angular harmonics $\exp(i(n + 2)\varphi)$, $\exp(i(n - 2)\varphi)$, $\exp(i(n + 1)\varphi)$, and $\exp(i(n - 1)\varphi)$. Therefore, the initial energy (power) of the beam (1) is divided into five parts. The power of each of these optical vortices was obtained in [14]. Let us find the polarization of these vortices. From (2), it can be seen that optical vortices with topological charges $(n + 1)$ and $(n - 1)$ have linear polarization, but the linear polarization vector is directed along the optical axis. That is, these vortices propagate along the plane of focus without crossing it. Therefore, these two vortices do not contribute to the longitudinal projection of the spin angular momentum (SAM), which shows the presence of elliptical or circular polarization in the beam cross section. The longitudinal projection of the SAM is determined (up to a constant) by the expression, which includes only the transverse projections of the light field (2):

$$S_z = 2\text{Im}\{E_x^* E_y\}.
 \tag{4}$$

Therefore, we consider the polarization of harmonics with topological charges $n, n + 2$, and $n - 2$. From (2), it follows that the Jones vectors for these optical vortices have the form:

$$e^{in\varphi} I_{0,n} \begin{pmatrix} 1 \\ 0 \end{pmatrix}, \quad \frac{1}{2} e^{i(n+2)\varphi} I_{2,n+2} \begin{pmatrix} 1 \\ -i \end{pmatrix}, \quad \frac{1}{2} e^{i(n-2)\varphi} I_{2,n-2} \begin{pmatrix} 1 \\ i \end{pmatrix}.
 \tag{5}$$

It can be seen from (5) that the initial optical vortex with topological charge n has retained its linear polarization at the focus, and additional vortices have circular polarization: the vortex with topological charge $(n + 2)$ has left-hand circular polarization, and the vortex with topological charge $(n - 2)$ has right circular polarization. But since their amplitudes

are different, the superposition of these vortices will have elliptical polarization. The sum of three optical vortices in (5) can be represented as:

$$\begin{aligned}
 & e^{in\varphi} I_{0,n} \begin{pmatrix} 1 \\ 0 \end{pmatrix} + \frac{1}{2} e^{i(n+2)\varphi} I_{2,n+2} \begin{pmatrix} 1 \\ -i \end{pmatrix} + \frac{1}{2} e^{i(n-2)\varphi} I_{2,n-2} \begin{pmatrix} 1 \\ i \end{pmatrix} = \\
 & \frac{e^{in\varphi}}{2} \left[\begin{pmatrix} 2I_{0,n} \\ 0 \end{pmatrix} + \cos(2\varphi) \begin{pmatrix} A \\ -iB \end{pmatrix} + i \sin(2\varphi) \begin{pmatrix} B \\ -iA \end{pmatrix} \right], \tag{6} \\
 & A = I_{2,n+2} + I_{2,n-2}, \quad B = I_{2,n+2} - I_{2,n-2}.
 \end{aligned}$$

It should be noted that since the energy contribution of the first term in the superposition for E_x in (2) and (6) is much greater than that of the second and third terms [14], the topological charge of the entire superposition E_x is equal to the topological charge of the optical vortex with a larger amplitude. This means the topological charge of the vortex field E_x in (2) and (6) is equal to n . However, despite the small amplitude of the second and third terms in (6), these terms will significantly affect the spin, which is proportional to the product (4) of all terms in (6). Similarly, the topological charge E_y in (2) and (6) will be equal to $n - 2$ ($n > 0$).

It can be seen from (6) that if $B > 0$, then at $\varphi = 0, \pi$ (on the horizontal axis) there will be left elliptical polarization, since instead of (6) we obtain:

$$\frac{(\pm 1)^n}{2} \begin{pmatrix} 2I_{0,n} + A \\ -iB \end{pmatrix}. \tag{7}$$

For $\varphi = \pi/2, 3\pi/2$ (vertical axis), instead of (6), we obtain the right elliptical polarization:

$$\frac{(\pm i)^n}{2} \begin{pmatrix} 2I_{0,n} - A \\ iB \end{pmatrix} \tag{8}$$

because near the optical axis $2I_{0,n} > I_{2,n+2} + I_{2,n-2}$. And vice versa, if $B < 0$, then on the horizontal axis at $\varphi = 0, \pi$ instead of (6), we obtain the right elliptical polarization:

$$\frac{(\pm 1)^n}{2} \begin{pmatrix} 2I_{0,n} + A \\ i|B| \end{pmatrix} \tag{9}$$

and on the vertical axis at $\varphi = \pi/2, 3\pi/2$, instead of (6), we obtain the left elliptical polarization:

$$\frac{(\pm i)^n}{2} \begin{pmatrix} 2I_{0,n} - A \\ -i|B| \end{pmatrix}. \tag{10}$$

Thus, due to the fact that the initial field in the form of an optical vortex with linear polarization after the spherical lens formed additional optical vortices with different amplitudes and with left and right circular polarizations, when three optical vortices are added in the focus plane, they form, at certain radii from optical axis, four local areas (two each on the vertical and horizontal axes of Cartesian coordinates), in which the left and right elliptical polarizations will be separated in pairs. That is, the spin Hall effect will take place at the focus. Note that at $n = 0$ (no optical vortex) in (6), the additional vortex harmonics $\exp(i2\varphi)$ and $\exp(-i2\varphi)$ will have the same amplitudes $I_{2,2} = I_{2,-2}$, and therefore there will be no spin Hall effect at the focus.

Substituting (2) into (4), we obtained the axial SAM component at the focus for the field (1):

$$S_z = \frac{1}{2} (I_{2,n-2} - I_{2,n+2})(I_{2,n-2} + I_{2,n+2} + 2 \cos(2\varphi) I_{0,n})$$

If the longitudinal projection of the SAM in the focal plane is positive, then the projection of the vector perpendicular to the plane of the polarization ellipse onto the optical axis is also positive. This means that the polarization vector rotates counterclockwise, as in the case of right-handed elliptical polarization. Otherwise, if the longitudinal projection

of the SAM in the focal plane is negative, then the vector perpendicular to the plane of the polarization ellipse has a negative projection on the optical axis. This means that the polarization vector rotates clockwise, as in the case of left-handed elliptical polarization. Due to the fact that the polarization ellipses in the focal plane are inclined and do not lie in the focal plane itself, the right-hand and left-hand rotation of the polarization vector in these ellipses does not change. Therefore, in order to establish the presence of the spin Hall effect at a tight focus, we do not need to consider the transverse projections of the SAM vector, S_x and S_y ; it is enough to determine the sign of the longitudinal projection S_z .

3. Reverse Energy Flux at the Focus of an Optical Vortex with Linear Polarization

It also follows from Equation (2) that not all the initial energy flux will cross the focus plane in the direction of light propagation, because part of the energy will propagate along the focus plane, and part of the energy will cross the focus plane in the opposite direction. Substituting the projections of the electromagnetic field (2) into the well-known expression for the Poynting vector, written up to a constant $\mathbf{P} = \text{Re}(\mathbf{E}^* \times \mathbf{H})$, where \mathbf{E} and \mathbf{H} are the electric and magnetic fields, the signs “*” and “ \times ” mean complex conjugation and vector product, and Re is the real part of the complex number, we obtain an expression for the longitudinal component of the energy flux at the field focus (1):

$$P_z = \frac{1}{2} \left(2I_{0,n}^2 - I_{2,n+2}^2 - I_{2,n-2}^2 \right). \tag{11}$$

The longitudinal projection of the energy flux at different radii r can be positive or negative, since the terms in (11) have different signs. On those circles centered on the optical axis, where $P_z < 0$, the energy flow flows in the opposite direction. It can be shown [14] that the total energy at the focus of each term in P_z is equal to the expression:

$$W_{v,\mu} = 2\pi \int_0^\infty |I_{v\mu}(r)|^2 r dr = 4\pi f^2 \int_0^a \sin^{2v+1} \left(\frac{\theta}{2} \right) \cos^{5-2v} \left(\frac{\theta}{2} \right) |A^*(\theta)|^2 d\theta = W_v. \tag{12}$$

It can be seen from (12) that the energy (or power) does not depend on the number of the Bessel function μ , which is included in the integrals (3). Applying Equation (12) to the total axial energy flux that crosses the focus plane from left to right and which has density (11), we obtain:

$$\hat{P}_z = \int_0^\infty r dr \int_0^{2\pi} d\varphi P_z(r) = W_0 - W_2 = W - 2W_1 - 2W_2. \tag{13}$$

In Equation (13), W is the total beam power, which is equal to $W = W_0 + W_2 + 2W_1$ [14]. It can be seen from (13) that the longitudinal energy flow is the sum of the direct energy flux equal to the total beam power W minus the energy flux $2W_1$ of two vortex harmonics $\exp(i(n + 1)\varphi)$ and $\exp(i(n - 1)\varphi)$, which have only a longitudinal projection of the electric field E_z and therefore propagate along the plane of focus and do not intersect it and minus the energy flux $2W_2$ of the other two vortex harmonics $\exp(i(n + 2)\varphi)$ and $\exp(i(n - 2)\varphi)$, which propagate in the opposite direction, crossing the plane of focus from right to left. The last statement follows from Equation (2). In (2), in the expression for E_x , both harmonics $\exp(i(n + 2)\varphi)$ and $\exp(i(n - 2)\varphi)$ enter with a plus, and they enter the expression for H_y with a minus. Therefore, the trio of vectors \mathbf{E}_x , \mathbf{H}_y , and $\mathbf{k}_z < 0$, where \mathbf{k}_z is the axial projection of the wave vector, describing the propagation of these two harmonics, is a right triple, where the projection onto the z -axis of the wave vector is negative. Similarly, from (2), it can be seen that in the expressions for E_y and H_x , both vortex harmonics $\exp(i(n + 2)\varphi)$ and $\exp(i(n - 2)\varphi)$ enter with the same signs; that is, the triple of vectors \mathbf{E}_y , \mathbf{H}_x , and $\mathbf{k}_z < 0$ are also the right trio of vectors, and therefore, these vortex harmonics propagate in the opposite direction of the z -axis.

On the other hand, the Poynting vector at the field focus (1) has, in addition to the longitudinal component P_z , the azimuthal component of the transverse energy flux P_φ . Therefore, we can assume that the total transverse (azimuthal) energy flux is equal to the sum of the last two terms in (13):

$$\hat{P}_\varphi = \int_0^\infty r dr \int_0^{2\pi} d\varphi P_\varphi(r) = 2(W_1 + W_2). \tag{14}$$

Expression (14) is obtained from the energy flux conservation law. However, it is not possible to directly integrate the azimuthal energy flux density. In [19], the azimuthal component of the Poynting vector at the focus of the field (1) was found (the radial component is equal to zero):

$$\begin{aligned} P_r &= 0, \\ P_\varphi &= I_{1,n+1}(I_{0,n} + I_{2,n+2}) + I_{1,n-1}(I_{0,n} + I_{2,n-2}). \end{aligned} \tag{15}$$

It can be seen from (15) that the transverse energy flux at the field focus (1) has only an azimuthal projection and rotates around the optical axis either counterclockwise ($P_\varphi > 0$) or clockwise ($P_\varphi < 0$).

4. Multiple Order Spin Hall Effect at the Focus of a Cylindrical Vector Beam with an Optical Vortex

In this section, we investigate the mechanism of the formation of the spin Hall effect at the focus of a more complex light field, which has both phase and polarization singularities in the initial plane. The Jones vector of such a light field in the initial plane has the form:

$$\begin{aligned} \mathbf{E}_{m,n}(\theta, \varphi) &= A(\theta) \exp(im\varphi) \begin{pmatrix} \cos n\varphi \\ \sin n\varphi \end{pmatrix}, \\ \mathbf{H}_{m,n}(\theta, \varphi) &= A(\theta) \exp(im\varphi) \begin{pmatrix} -\sin n\varphi \\ \cos n\varphi \end{pmatrix}. \end{aligned} \tag{16}$$

For light field (16), in contrast to the light field (1), the topological charge is designated as m , and the order of the cylindrical vector beam (16) is designated as n . We used these notations so that the Equations (6) and (19) are similar to each other.

The distribution of all projections of the electric and magnetic fields in a tight focus has already been found in [20]. Here, without derivation, we present these projections for the convenience of readers:

$$\begin{aligned} E_x &= \frac{i^{m+n-1}}{2} e^{i(m+n)\varphi} (I_{0,m+n} + e^{-2i\varphi} I_{2,m+n-2}) + \frac{i^{m-n-1}}{2} e^{i(m-n)\varphi} (I_{0,m-n} + e^{2i\varphi} I_{2,m-n+2}), \\ E_y &= \frac{i^{m+n}}{2} e^{i(m+n)\varphi} (-I_{0,m+n} + e^{-2i\varphi} I_{2,m+n-2}) + \frac{i^{m-n}}{2} e^{i(m-n)\varphi} (I_{0,m-n} - e^{2i\varphi} I_{2,m-n+2}), \\ E_z &= i^{m+n} e^{i(m+n-1)\varphi} I_{1,m+n-1} - i^{m-n} e^{i(m-n+1)\varphi} I_{1,m-n+1}, \\ H_x &= \frac{i^{m+n}}{2} e^{i(m+n)\varphi} (I_{0,m+n} + e^{-2i\varphi} I_{2,m+n-2}) - \frac{i^{m-n}}{2} e^{i(m-n)\varphi} (I_{0,m-n} + e^{2i\varphi} I_{2,m-n+2}), \\ H_y &= \frac{i^{m+n-1}}{2} e^{i(m+n)\varphi} (I_{0,m+n} - e^{-2i\varphi} I_{2,m+n-2}) + \frac{i^{m-n-1}}{2} e^{i(m-n)\varphi} (I_{0,m-n} - e^{2i\varphi} I_{2,m-n+2}), \\ H_z &= i^{m+n+1} e^{i(m+n-1)\varphi} I_{1,m+n-1} + i^{m-n+1} e^{i(m-n+1)\varphi} I_{1,m-n+1}, \end{aligned} \tag{17}$$

In the initial plane, the light field (16) has a linear polarization at each point of the beam cross section, and such a field can be represented as a superposition of two optical vortices with topological charges $m + n$ and $m - n$ with left and right circular polarizations with the same amplitude modules:

$$e^{im\varphi} \begin{pmatrix} \cos n\varphi \\ \sin n\varphi \end{pmatrix} = \frac{1}{\sqrt{2}} e^{i(m+n)\varphi} \begin{pmatrix} 1 \\ -i \end{pmatrix} + \frac{1}{\sqrt{2}} e^{i(m-n)\varphi} \begin{pmatrix} 1 \\ i \end{pmatrix}. \tag{18}$$

Then, as follows from (17), in the plane of focus, due to refraction on the surface of a spherical lens, additional optical vortices appear with topological charges $m + n - 2$,

$m - n + 2$, $m + n - 1$, and $m - n + 1$. The Jones vector for the transverse components of the electric field at the focus, as follows from (17), has the form:

$$E_{\perp} = \frac{i^{m+n-1}}{2} e^{im\varphi} \left[\left(e^{i(n-2)\varphi} I_{2,m+n-2} + (-1)^n e^{-in\varphi} I_{2,m-n} \right) \begin{pmatrix} 1 \\ i \end{pmatrix} + \left(e^{-i(n-2)\varphi} (-1)^n I_{2,m-n+2} + e^{in\varphi} I_{2,m+n} \right) \begin{pmatrix} 1 \\ -i \end{pmatrix} \right]. \tag{19}$$

It can be seen from Equation (19) that the transverse light field at the focus is a superposition of two optical vortices with different amplitudes and left and right circular polarization. This means that when these fields are added, the regions with left and right elliptical polarizations will be in focus. It is known that for the sum of two scalar optical vortices with different topological charges p and q , the intensity distribution will have $|p - q|$ “chamomile” petals. In our case, the field with the right circular polarization will have $2n - 2$ lobes, and the field with the left circular polarization will also have $2n - 2$ lobes, but they will be located in different places. And since the fields with orthogonal polarization are added modulo, then in the focus of the field (19), there will be only $4n - 4$ side lobes of intensity, in which the polarization will alternate: left elliptical, then right elliptical. From (17), one can obtain the exact expression for the longitudinal projection of the spin density vector at the focus for field (16):

$$S_z = \text{Im}(E_x^* E_y) = \frac{1}{2} \left[I_{0,m-n}^2 - I_{0,m+n}^2 + I_{2,m+n-2}^2 - I_{2,m-n+2}^2 + 2(-1)^n \cos(2(n-1)\varphi) (I_{0,m-n} I_{2,m+n-2} - I_{0,m+n} I_{2,m-n+2}) \right]. \tag{20}$$

It can be seen from (20) that on a certain circle in the beam cross section at the focus centered on the optical axis, the longitudinal spin angular momentum (spin density) will change sign $4(n - 1)$ times, since the cosine argument changes sign over the period exactly that many times. Here, we have shown how regions with different spins are formed at the focus, and thus have shown that for field (16), the spin Hall effect takes place at the focus.

5. Numerical Simulation

Using the Richards–Wolf formula, we numerically simulated the focusing of a linearly polarized optical vortex (1) with an aplanatic lens (NA = 0.95). We assume focusing an initial plane wave $A(\theta) = 1$ of wavelength $\lambda = 532$ nm. Figures 1 and 2 show the distribution of module (a, c) and phase (b, d) of the electric field components E_x and E_y for optical vortices equal to $n = 1$ (Figure 1) and $n = 2$ (Figure 2).

Figure 1b,d show the phase values at four points on the Cartesian axes. If we compare these phase values in Figure 1b,d, it can be seen that on the vertical axis, the phase differences of the fields E_x and E_y will be equal to $-\pi/2$, and the phase differences along the horizontal axis will be equal to $\pi/2$. And since the amplitudes of the fields E_x (Figure 1a) and E_y (Figure 1c) are different, along the vertical axis at these points, there will be a right elliptical polarization, and along the horizontal axis at these points, there will be a left elliptical polarization. The topological charge in Figure 1b is equal to 1, and in Figure 1d it is equal to -1 .

Figure 2b,d show the phase values at four points on the Cartesian axes (and center). If we compare these phase values in Figure 2b,d, it can be seen that on the vertical axis, the phase differences of the fields E_x and E_y will be equal to $-\pi/2$, and the phase differences along the horizontal axis will be equal to $\pi/2$. And since the amplitudes of the fields E_x (Figure 2a) and E_y (Figure 2c) are different, on the vertical axis at these points, there will be a right elliptical polarization, and on the horizontal axis at these points, there will be a left elliptical polarization. From Figures 1 and 2, it follows that in both cases in the focal plane, there are regions with the centers located on the Cartesian axes, in which the elliptical polarization has different signs. On the vertical axis, the polarization vector rotates counterclockwise, and on the horizontal axis, it rotates counterclockwise. The topological charge in Figure 2b is equal to 2, and in Figure 2d it is equal to 0.

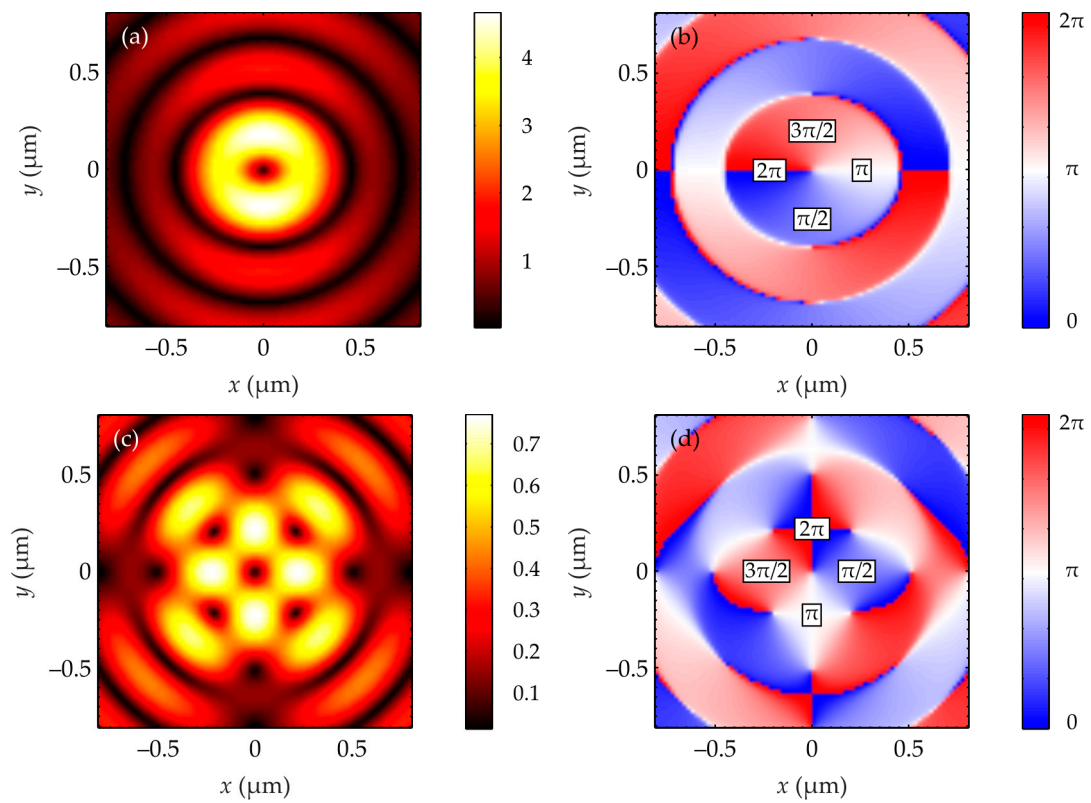


Figure 1. Distribution of the modulus (a,c) and phase (b,d) of electric field components E_x (a,b) and E_y (c,d) for the linearly polarized optical vortex with a topological charge of $n = 1$.

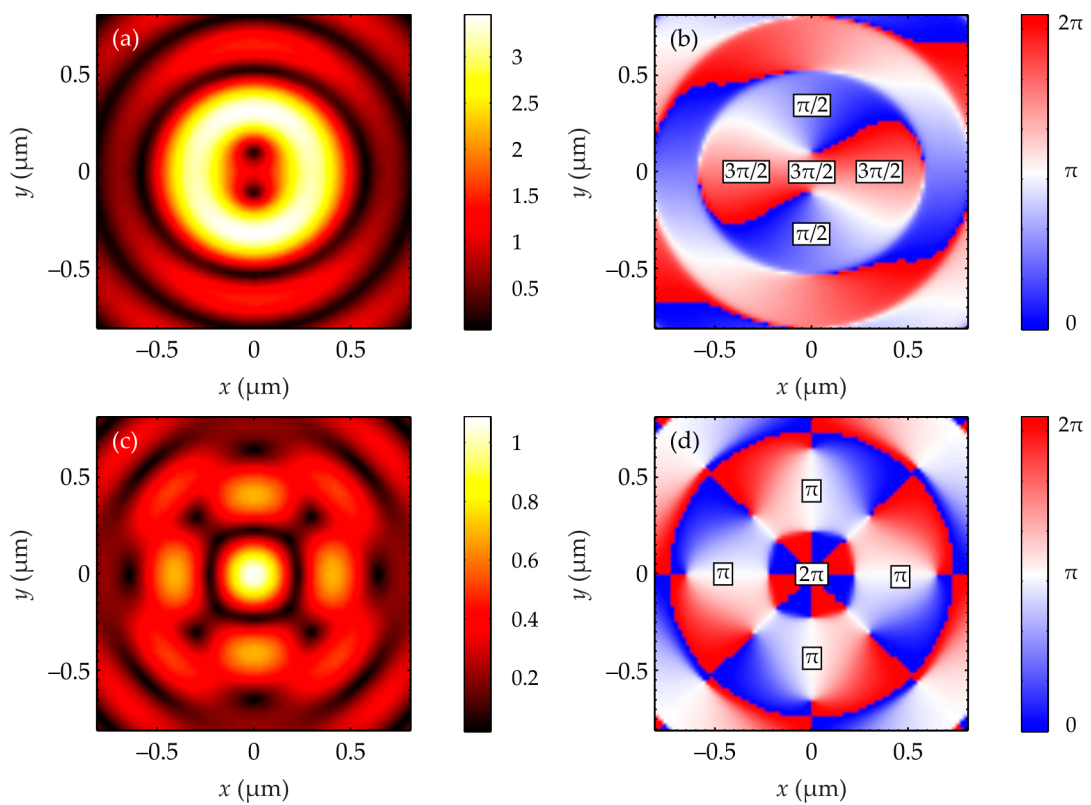


Figure 2. Distribution of the modulus (a,c) and phase (b,d) of electric field components E_x (a,b) and E_y (c,d) for the linearly polarized optical vortex with a topological charge of $n = 2$.

Figures 3 and 4 show the distribution of the module and phase of the electric field components E_x and E_y for cylindrical vector beams (16) with optical vortices equal to $m = 1$ (Figure 3) and $m = 2$ (Figure 4).

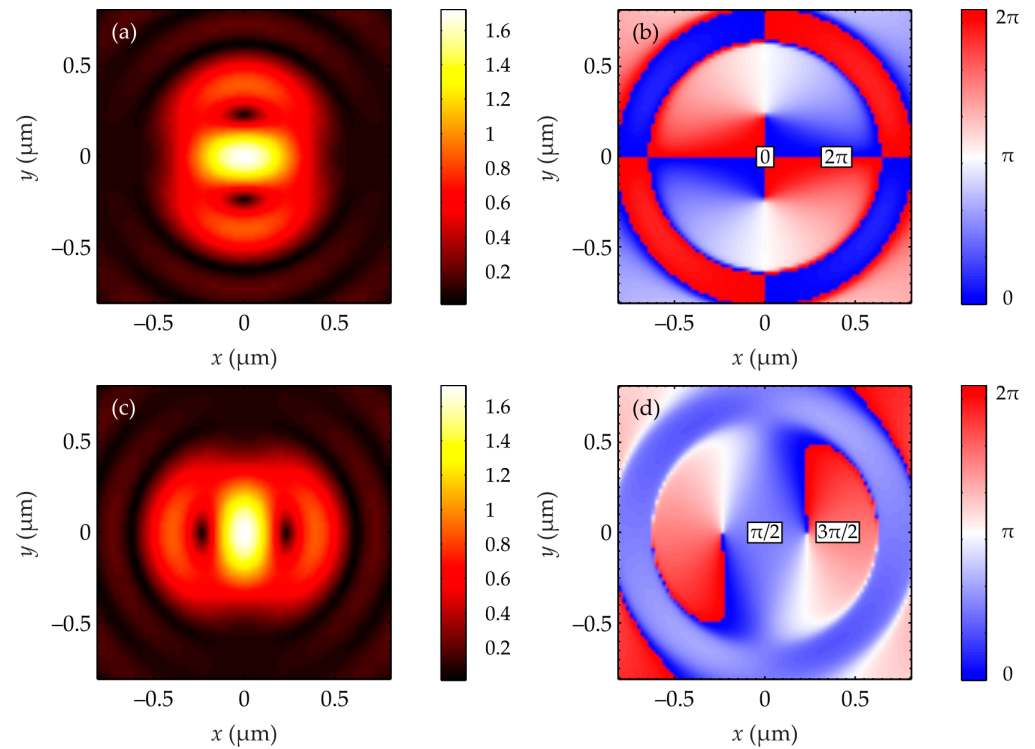


Figure 3. Distribution of the modulus (a,c) and phase (b,d) of electric field components E_x (a,b) and E_y (c,d) for the cylindrical vector beam $n = 1$ with an optical vortex of a topological charge of $m = 1$.

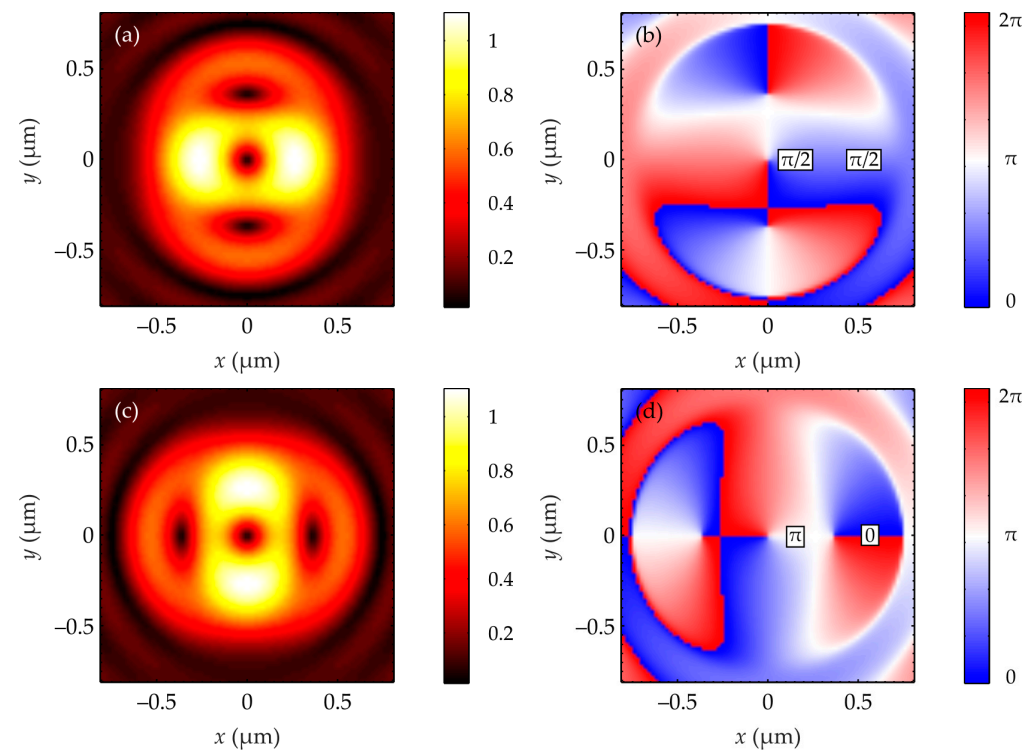


Figure 4. Distribution of the modulus (a,c) and phase (b,d) of electric field components E_x (a,b) and E_y (c,d) for the cylindrical vector beam $n = 1$ with an optical vortex of a topological charge of $m = 2$.

From Equation (20) it follows that for $n = 1$, the spin density at the focus of (16) will have radial symmetry. It depends on the radial variable only. Therefore, Figure 3b,d show the phase values at two points on the horizontal axis. If we compare these phase values in Figure 3b,d, it can be seen that at the center, the phase difference of the fields E_x and E_y will be equal to $-\pi/2$, and the phase difference at some distance from the center will be equal to $\pi/2$. Since the amplitudes of the fields E_x (Figure 3a) and E_y (Figure 3c) are different, in the center (on the optical axis), there will be a right elliptical polarization, and on a circle of a certain radius, there will be a left elliptical polarization. The topological charge in Figure 3b is equal to 0, and in Figure 3d, it is equal to 0.

Similarly, if we compare the phase values in Figure 4b,d, we can see that at the center, the phase difference of the fields E_x and E_y will be equal to $-\pi/2$, and the phase difference at some distance from the center will be equal to $\pi/2$. Since the amplitudes of the fields E_x (Figure 4a) and E_y (Figure 4c) are different, in the center (on the optical axis), there will be a right elliptical polarization, and on a circle of a certain radius, there will be a left elliptical polarization. The topological charge in Figure 4b is equal to 1, and in Figure 4d, it is equal to 1.

Figure 5 shows the distributions of the SAM at the focus of the beam (1) with topological charge $n = 1$ (Figure 5a) and topological charge $n = 2$ (Figure 5b) and at the focus of a cylindrical vector beam (16) of order $n = 1$ with topological charge $m = 1$ (Figure 5c) and topological charge $m = 2$ (Figure 5d). Figure 5 confirms the distribution of regions with left and right elliptical polarizations that follow from the discussion of Figures 1–4. At the focus of (1), regardless of the topological charge n , the regions with the right elliptical polarization are located along the vertical Cartesian axis, and the regions with the left elliptical polarization are located along the horizontal Cartesian axis (Figure 5a,b). At the focus of a cylindrical vector beam (16) of order $n = 1$ for any topological charge m , regions with different signs of the SAM (with different directions of rotation of the elliptical polarization vector) will be located on circles with different radii (Figure 5c,d).

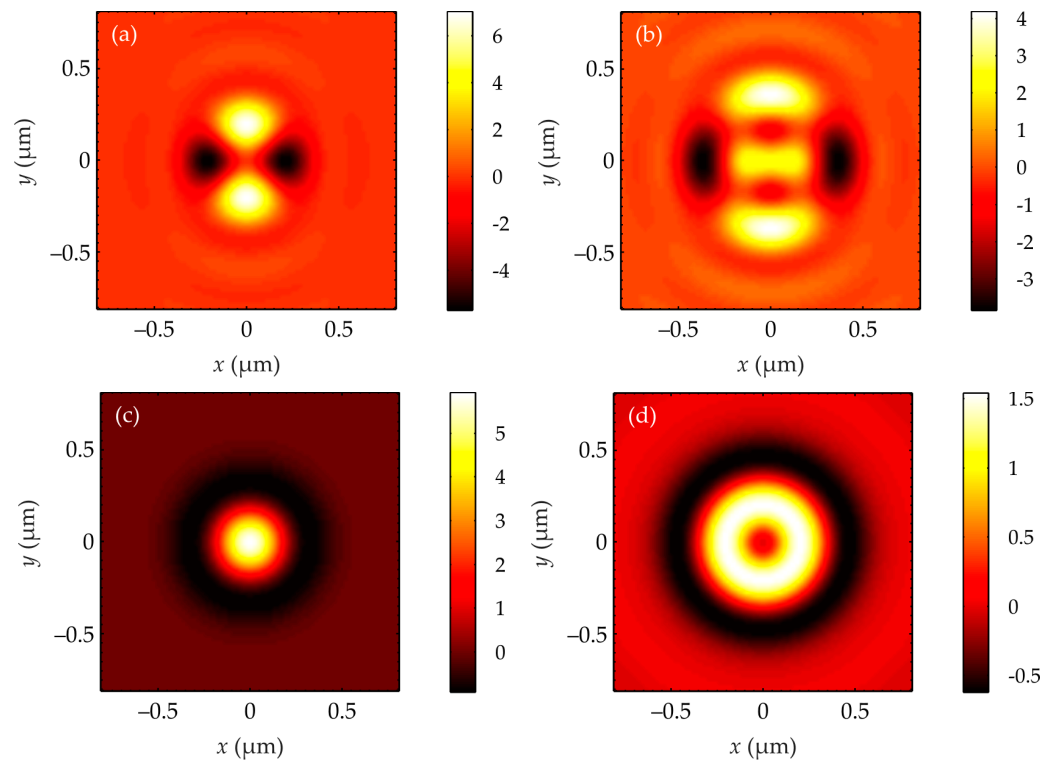


Figure 5. SAM for the tightly focused linearly polarized optical vortex with a topological charge of $n = 1$ (a) and $n = 2$ (b) and for the tightly focused cylindrical vector beam $n = 1$ with an optical vortex of a topological charge of $m = 1$ (c) and $m = 2$ (d).

Figure 6 shows the distribution of the SAM (Figure 5), normalized to the intensity in the focal plane:

$$S_z = \frac{2\text{Im}(E_x^*E_y)}{E_x^*E_x + E_y^*E_y}. \quad (21)$$

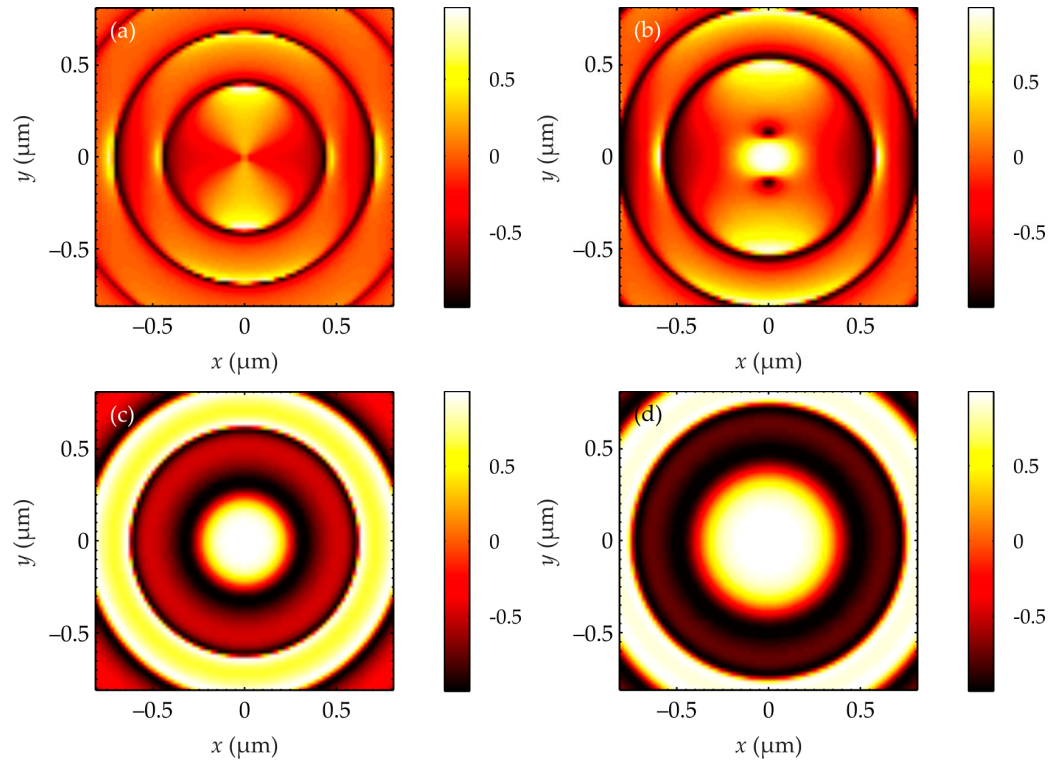


Figure 6. Normalized SAM for the tightly focused linearly polarized optical vortex with a topological charge of $n = 1$ (a) and $n = 2$ (b) and for the tightly focused cylindrical vector beam $n = 1$ with an optical vortex of a topological charge of $m = 1$ (c) and $m = 2$ (d).

6. Discussion

Thus, in this paper, using two vortex beams with uniform (1) and inhomogeneous linear polarization (16), we have shown how the spin Hall effect is formed in a tight focus. We have shown that for these light fields (1) and (16), additional optical vortices are formed at the focus with different amplitudes and with left and right circular polarization (5). The superposition of these additional vortices forms regions located either on the Cartesian axes (Figure 5a,b) or on circles of different radii (Figure 5c,d), in which the elliptical polarization of different signs (left or right) takes place. In both cases, (1) and (16), the initial field had no SAM ($S_z = 0$). But as the fields (1) and (16) propagate in free space after the spherical lens, subwavelength regions with spins of different signs are formed at the focus. In this case, the total spin at the focus (the spin density (4) averaged over the beam cross section) is still equal to zero. The question remains: why and at what moment are additional optical vortices formed? The answer to this question can be found in the Richards–Wolf theory [18]. If before the spherical lens the transverse projections of the field were equal to $E_{x,0}$ and $E_{y,0}$, then immediately after the spherical lens, these projections are transformed according to the expression:

$$\begin{pmatrix} E_x \\ E_y \end{pmatrix} = \begin{pmatrix} 1 + A(\theta) \cos^2 \varphi & 0.5A(\theta) \sin 2\varphi \\ 0.5A(\theta) \sin 2\varphi & 1 + A(\theta) \sin^2 \varphi \end{pmatrix} \begin{pmatrix} E_{x,0} \\ E_{y,0} \end{pmatrix}, \quad A(\theta) = \cos \theta - 1, \quad (22)$$

where θ and φ are the polar and azimuthal angles in a coordinate system with the center at the focus. It can be seen from (22) that the transformation matrix contains the squares of the

cosine and sine of the azimuthal angle, which are responsible for the formation of additional vortices with topological charges equal to $n + 2$ and $n - 2$. However, immediately after the spherical lens, these additional optical vortices with left and right circular polarization have equal amplitudes, and therefore, their superposition has linear polarization. Optical vortices with different topological charges are divergent differently due to diffraction in free space. Therefore, during the propagation, these additional optical vortices acquire different amplitudes, and their superposition forms an elliptical polarization of different signs. That is, immediately after the spherical lens, the Hall effect is absent and has a maximum value in the plane of focus. Between the spherical lens and the focus, the spin Hall effect has an intermediate value from zero to a maximum.

The Hall effect can be estimated from the value of the normalized SAM (21). The closer the modulus S_z is to 1, the stronger the spin Hall effect. Also, the magnitude of the Hall effect is affected by the ratio of light energy at the focus, which falls in regions with spins of different signs, to the total energy of the beam at the focus.

It should be noted that the spin Hall effect, which appears as a transverse displacement by small fractions of the wavelength of reflected beams with left and right circular polarization from the interface between two media [21] or from a metasurface [22], is difficult to measure. However, there are already attempts to use this effect to differentiate optical signals and to enhance the edges of the image [21,22]. The Hall effect arising at a sharp focus is much easier to detect by measuring the third Stokes component. For example, in Figure 6, in the plane of focus in a region of about 300 nm in size, the third Stokes component (21) is equal to 0.5, and in an adjacent region of the same size, it is equal to -0.5 . The authors plan to carry out such experimental measurements. The spin Hall effect at a sharp focus can be used for the subwavelength magnetization of materials using the inverse Faraday effect [23] or for structuring the surface of polarization-sensitive materials [24].

It should also be noted that the optical Magnus effect is closely related to the optical spin Hall effect [25]. In [25], it was experimentally shown that an optical vortex with circular polarization, propagating in a uniaxial crystal at an angle to the optical axis, splits into two beams, one of which is displaced in the direction perpendicular to the tilt plane.

7. Conclusions

In this paper, we have shown theoretically and numerically that in a tightly focused cylindrical vector beam of order n with an embedded optical vortex with a topological charge of m (16), there are six optical vortices: two with topological charges $m + n - 2$ and $m - n$ with right-hand circular polarization, two with topological charges $m - n + 2$ and $m + n$ and with left-hand circular polarization (19), and two with topological charges $m + n - 1$ and $m - n + 1$ with linear polarization directed along the optical axis (17). The last two optical vortices do not contribute to the longitudinal projection of the spin angular momentum vector, which is proportional to the third Stokes component and indicates the existence of right-hand or left-hand circular polarizations in the focal plane. Optical vortices with left and right circular polarization have different amplitudes in the focal plane, due to the fact that optical vortices with different topological charges diverge differently in space. Due to the different amplitudes of optical vortices, their spins of different signs are not compensated in summation. Therefore, regions with positive and negative spin (regions with left and right elliptical polarization), or, in other words, with a positive and negative longitudinal projection of the SAM (21), are formed in the focal plane. When $n = 1$ (Figure 6c,d), the distribution of the longitudinal projection of the SAM has circular symmetry. The separation of photons with different spins in space is called the optical spin Hall effect.

Author Contributions: Conceptualization, V.V.K.; methodology, V.V.K. and A.M.T.; software, S.S.S.; validation, S.S.S. and A.M.T.; formal analysis, V.V.K. and E.S.K.; investigation, V.V.K. and S.S.S.; resources, S.S.S. and A.M.T.; data curation, S.S.S. and E.S.K.; writing—original draft preparation, V.V.K.; writing—review and editing, V.V.K.; visualization, S.S.S. and A.M.T.; supervision, V.V.K.;

project administration, V.V.K.; funding acquisition, V.V.K. All authors have read and agreed to the published version of the manuscript.

Funding: This work was supported by the Russian Science Foundation (Project No. 23-12-00236) in simulation and the Ministry of Science and Higher Education within the State assignment FSRC «Crystallography and Photonics» RAS in theory.

Institutional Review Board Statement: Not applicable.

Informed Consent Statement: Not applicable.

Data Availability Statement: Data underlying the results presented in this paper may be obtained from the authors upon reasonable request.

Acknowledgments: This work was supported by the Russian Science Foundation (Project No. 23-12-00236) in part of “Simulation” and the Ministry of Science and Higher Education within the State assignment FSRC «Crystallography and Photonics» RAS in part of “Theory”.

Conflicts of Interest: The authors declare no conflict of interest.

References

1. Onoda, M.; Murakami, S.; Nagaosa, N. Hall Effect of Light. *Phys. Rev. Lett.* **2004**, *93*, 083901. [[CrossRef](#)] [[PubMed](#)]
2. Bliokh, K.Y.; Bliokh, Y.P. Conservation of Angular Momentum, Transverse Shift, and Spin Hall Effect in Reflection and Refraction of an Electromagnetic Wave Packet. *Phys. Rev. Lett.* **2006**, *96*, 073903. [[CrossRef](#)] [[PubMed](#)]
3. Kavokin, A.; Malpuech, G.; Glazov, M. Optical Spin Hall Effect. *Phys. Rev. Lett.* **2005**, *95*, 136601. [[CrossRef](#)]
4. Leyder, C.; Romanelli, M.; Karr, J.P.; Giacobino, E.; Liew, T.C.H.; Glazov, M.M.; Kavokin, A.V.; Malpuech, G.; Bramati, A. Observation of the optical spin Hall effect. *Nat. Phys.* **2007**, *3*, 628–631. [[CrossRef](#)]
5. Kim, M.; Lee, D.; Kim, T.H.; Yang, Y.; Park, H.J.; Rho, J. Observation of Enhanced Optical Spin Hall Effect in a Vertical Hyperbolic Metamaterial. *ACS Photonics* **2019**, *6*, 2530–2536. [[CrossRef](#)]
6. Liu, Y.; Ke, Y.; Luo, H.; Wen, S. Photonic spin Hall effect in metasurfaces: A brief review. *Nanophotonics* **2017**, *6*, 51–70. [[CrossRef](#)]
7. Yin, X.; Ye, Z.; Rho, J.; Wang, Y.; Zhang, X. Photonic Spin Hall Effect at Metasurfaces. *Science* **2013**, *339*, 1405–1407. [[CrossRef](#)]
8. Liu, S.; Chen, S.; Wen, S.; Luo, H. Photonic spin Hall effect: Fundamentals and emergent applications. *Opto-Electron. Sci.* **2022**, *1*, 220007. [[CrossRef](#)]
9. Luo, H.; Wen, S.; Shu, W.; Tang, Z.; Zou, Y.; Fan, D. Spin Hall effect of a light beam in left-handed materials. *Phys. Rev. A* **2009**, *80*, 043810. [[CrossRef](#)]
10. Luo, H.; Ling, X.; Zhou, X.; Shu, W.; Wen, S.; Fan, D. Enhancing or suppressing the spin Hall effect of light in layered nanostructures. *Phys. Rev. A* **2011**, *84*, 033801. [[CrossRef](#)]
11. Zhou, X.; Ling, X.; Luo, H.; Wen, S. Identifying graphene layers via spin Hall effect of light. *Appl. Phys. Lett.* **2012**, *101*, 251602. [[CrossRef](#)]
12. Cai, L.; Liu, M.; Chen, S.; Liu, Y.; Shu, W.; Luo, H.; Wen, S. Quantized photonic spin Hall effect in graphene. *Phys. Rev. A* **2017**, *95*, 013809. [[CrossRef](#)]
13. Zhou, X.; Zhang, J.; Ling, X.; Chen, S.; Luo, H.; Wen, S. Photonic spin Hall effect in topological insulators. *Phys. Rev. A* **2013**, *88*, 053840. [[CrossRef](#)]
14. Kovalev, A.A.; Kotlyar, V. V Spin Hall Effect of Double-Index Cylindrical Vector Beams in a Tight Focus. *Micromachines* **2023**, *14*, 494. [[CrossRef](#)] [[PubMed](#)]
15. Li, H.; Ma, C.; Wang, J.; Tang, M.; Li, X. Spin-orbit Hall effect in the tight focusing of a radially polarized vortex beam. *Opt. Express* **2021**, *29*, 39419. [[CrossRef](#)]
16. Shu, W.; Lin, C.; Wu, J.; Chen, S.; Ling, X.; Zhou, X.; Luo, H.; Wen, S. Three-dimensional spin Hall effect of light in tight focusing. *Phys. Rev. A* **2020**, *101*, 23819. [[CrossRef](#)]
17. Kovalev, A.A.; Kotlyar, V.V.; Stafeev, S.S. Spin Hall Effect in the Paraxial Light Beams with Multiple Polarization Singularities. *Micromachines* **2023**, *14*, 777. [[CrossRef](#)]
18. Richards, B.; Wolf, E. Electromagnetic Diffraction in Optical Systems. II. Structure of the Image Field in an Aplanatic System. *Proc. R. Soc. A Math. Phys. Eng. Sci.* **1959**, *253*, 358–379. [[CrossRef](#)]
19. Kotlyar, V.V.; Nalimov, A.G.; Stafeev, S.S. Exploiting the circular polarization of light to obtain a spiral energy flow at the subwavelength focus. *J. Opt. Soc. Am. B* **2019**, *36*, 2850–2855. [[CrossRef](#)]
20. Kotlyar, V.V.; Stafeev, S.S.; Kovalev, A.A. Reverse and toroidal flux of light fields with both phase and polarization higher-order singularities in the sharp focus area. *Opt. Express* **2019**, *27*, 16689–16702. [[CrossRef](#)]
21. Ji, Y.W.; Ma, X.K.; Hu, H.J.; Li, X.Z. Enhanced edge detection based on spin hall effect in the uniaxial crystal. *Front. Phys.* **2022**, *10*, 862156. [[CrossRef](#)]
22. Zhang, J.; Zhou, S.; Dai, X.; Huang, M.; Yu, X. All-optical image edge detection based on the two-dimensional photonic spin Hall effect in anisotropic metamaterial. *Opt. Express* **2023**, *31*, 6062–6075. [[CrossRef](#)] [[PubMed](#)]

23. Merte, M.; Freimuth, F.; Go, D.; Adamantopoulos, T.; Lux, F.R.; Plucinski, L.; Gomonay, O.; Blügel, S.; Mokrousov, Y. Photocurrents, inverse Faraday effect, and photospin Hall effect in Mn₂Au. *APL Mater.* **2023**, *11*, 071106. [[CrossRef](#)]
24. Zhai, Y.; Cao, L.; Liu, Y.; Tan, X. A Review of Polarization-Sensitive Materials for Polarization Holography. *Materials* **2020**, *13*, 5562. [[CrossRef](#)]
25. Fadeyeva, T.A.; Rubass, A.F.; Volyar, A.V. Transverse shift of a high-order paraxial vortex-beam induced by a homogeneous anisotropic medium. *Phys. Rev. A* **2009**, *79*, 053815. [[CrossRef](#)]

Disclaimer/Publisher's Note: The statements, opinions and data contained in all publications are solely those of the individual author(s) and contributor(s) and not of MDPI and/or the editor(s). MDPI and/or the editor(s) disclaim responsibility for any injury to people or property resulting from any ideas, methods, instructions or products referred to in the content.